this analysis did not include medial and orbital frontal regions; neither of these regions showed content-specific sustained activity.

24. In the right hemisphere, the differences between the spatial extents of sustained activation for face and spatial working memory were 6.1 and 3.3 cm³ and 0.31 and 0.23% signal change in the middle frontal cortex, and 1.8 and 1.8 cm³ and 0.39 and 0.25% in the inferior frontal cortex (medians across subjects; $P > 0.1$ for all comparisons).

25. Others (*2*, *4*, *20*) have also directly contrasted object and spatial working memory and, as we did, they found evidence for domain specificity in prefrontal cortex. However, their evidence indicated that domain specificity is primarily a hemispheric laterality effect, with left frontal regions specialized for object working memory and right frontal regions specialized for spatial working memory. In our previous studies of face (*7*, *14*) and in this study of spatial working memory, we found activations with similar coordinates, but the activations tended to be bilateral. Smith *et al.* (*2*) attributed the left lateralization of object working memory to rehearsal of a symbolically or linguistically encoded representation of the object. In this study and previously (*14*) we have seen left lateralization for face working memory under conditions that encouraged more symbolic or verbal encoding of faces, but we have also seen right lateralization under conditions that allowed for more image-based encoding (*14*, *15*). We argue that laterality effects in visual memory may be influenced

by a variety of factors, such as memory set size, retention interval length, and item familiarity, all of which may affect the extent to which subjects engage in symbolic or verbal encoding and rehearsal.

26. Whereas activation in the superior frontal sulcus was overwhelmingly associated with sustained activity during spatial working memory (89% of activated cortex), activation in the precentral sulcus was a mixture of voxels demonstrating sustained (53%) and transient (43%) activity during working memory as well as saccade-related activity (74%; median percentages for four subjects include overlap). The presence of both sustained and transient activity in the precentral sulcus at the level of the FEF is consistent with results of physiological studies in monkeys that have demonstrated that some FEF neurons show sustained activity during fixation or during the delays in memory-guided saccade tasks, and others show transient activity during saccadic and pursuit eye movements (*27*, *33*). Transient activity observed in the precentral sulcus is likely to be related to eye movements to the locations where pictures appeared, because subjects were instructed to look directly at each picture as it was shown and to avoid moving their eyes during delay periods. Regions of the precentral sulcus activated by the spatial working memory task but not by the saccadic eye movement task may be related to mechanisms of oculomotor control other than those controlling horizontal saccades. However, it is highly unlikely that sustained activity in the superior frontal sulcus is related to

oculomotor control because current and previous eye movement studies in humans have localized activity related to visually guided saccades, self-paced saccades, smooth pursuit, and fixation within or posterior to the precentral sulcus and not within the superior frontal sulcus (*17*, *18*).

27. S. Funahashi, C. J. Bruce, P. S. Goldman-Rakic, *J. Neurophysiol.* **61**, 331 (1989).
28. L. G. Ungerleider and J. V. Haxby *Curr. Opin. Neurobiol.* **4**, 157 (1994); L. G. Ungerleider, *Science* **270**, 769 (1995).
29. D. T. Stuss and D. F. Benson, *The Frontal Lobes* (Raven Press, New York, 1986).
30. C. J. Bruce and M. E. Goldberg, *J. Neurophysiol.* **53**, 603 (1985).
31. ———, *ibid.* **54**, 714 (1985).
32. G. B. Stanton, S.-Y. Deng, M. E. Goldberg, N. T. McMullen, *J. Comp. Neurol.* **282**, 415 (1989).
33. M. E. Goldberg and M. A. Segraves, in *The Neurobiology of Saccadic Eye Movements*, R. H. Wurtz and M. E. Goldberg, Eds. (Elsevier, Amsterdam, 1989), p. 283; J. P. Gottlieb *et al.*, *J. Neurophysiol.* **72**, 1634 (1994).
34. The authors thank R. Desimone and A. Martin for comments on an earlier draft of the manuscript; E. Hoffman and J. Schouten for help with subject recruitment, scheduling, and training; and P. Jezzard and the staff of the NIH In Vivo NMR Center for assistance with MR scanning.

Propagating Activity Patterns in Large-Scale Inhibitory Neuronal Networks

J. Rinzel,* D. Terman, X.-J. Wang, B. Ermentrout

The propagation of activity is studied in a spatially structured network model of γ-aminobutyric acid–containing (GABAergic) neurons exhibiting postinhibitory rebound. In contrast to excitatory-coupled networks, recruitment spreads very slowly because cells fire only after the postsynaptic conductance decays, and with two possible propagation modes. If the connection strength decreases monotonically with distance (on-center), then propagation occurs in a discontinuous manner. If the self- and nearby connections are absent (off-center), propagation can proceed smoothly. Modest changes in the synaptic reversal potential can result in depolarization-mediated waves that are 25 times faster. Functional and developmental roles for these behaviors and implications for thalamic circuitry are suggested.

Reciprocally inhibitory neural circuits are known to be a fundamental substrate for rhythmogenesis in animals' central pattern generator systems (*1*). Subnetworks of mutually connected neurons were also found in various systems of the mammalian brain,

such as the hippocampus, neocortex, and thalamus (*2*). The operation and significance of such interneuronal networks are not well understood. Recent studies showed that synaptic inhibition can synchronize cells, thereby contributing to the generation of large-scale rhythmic activities observed in the thalamus and hippocampus (*3–5*). Another possible function is disinhibition, where the interneurons projecting to a principal neuron are selectively inhibited by another group of interneurons. This mechanism would require specialized connectivity patterns between mutually inhibitory cells and with principal neurons (on-center or off-center), which are generally difficult to identify by anatomical and electrophysiological experiments. In the present work, we demonstrate by model simulations that the spatiotemporal activity patterns of

an interneuronal population display a number of unique dynamic features. The qualitative characteristics dramatically depend on, and therefore can subserve as predictive indicators of, the underlying synaptic circuit architecture.

As a specific example, the thalamocortical (TC) relay neurons receive powerful recurrent inhibition from GABAergic cells in the thalamic reticular nucleus (RE). How this feedback inhibition is organized spatially will determine in part its role in the sensory information processing within the thalamus (*6*). The RE-mediated synaptic inhibition is also critically involved in the generation of the synchronous thalamic spindle oscillations during light sleep (*3*). Moreover, in the thalamic slice models one finds spatiotemporally organized activity in the form of propagating waves, which are waves that move very slowly (~1 mm/s), on each cycle recruiting additional inactive cells in a distinctive, non-smooth, "lurching" manner (*7*, *8*). In this paper, we consider a spatially structured network of GABAergic neurons, which may be interpreted as a reduction from a two-population thalamic network. The idea is that because the TC-to-RE projection is topographic and acts via rapid glutamate receptors of the α-amino-3-hydroxy-5-methyl-4-isoxazolepropionic acid (AMPA) type, the excitation in a TC cell would result in a barrage of inhibitory postsynaptic potentials (IPSPs) in the neighboring TC cells (through the disynaptic TC-RE-TC loop). In this idealized view (of the isolated thalamic circuit), the TC cell layer acts ef-

J. Rinzel, Mathematical Research Branch, National Institute of Diabetes and Digestive and Kidney Diseases, National Institutes of Health, Bethesda, MD 20892, USA.
D. Terman, Department of Mathematics, Ohio State University, Columbus, OH 43210, USA.
X.-J. Wang, Center for Complex Systems and Department of Physics, Brandeis University, Waltham, MA 02254, USA.
B. Ermentrout, Department of Mathematics, University of Pittsburgh, Pittsburgh, PA 15260, USA.

*Present address: Center for Neural Science and Courant Institute of Mathematical Sciences, New York University, New York, NY 10003, USA. To whom correspondence should be addressed at the Center for Neural Science, 4 Washington Place, Room 809, New York University, New York, NY 10003, USA. E-mail: rinzel@cns.nyu.edu

fectively as a cell population with reciprocal GABAergic inhibitory interactions.
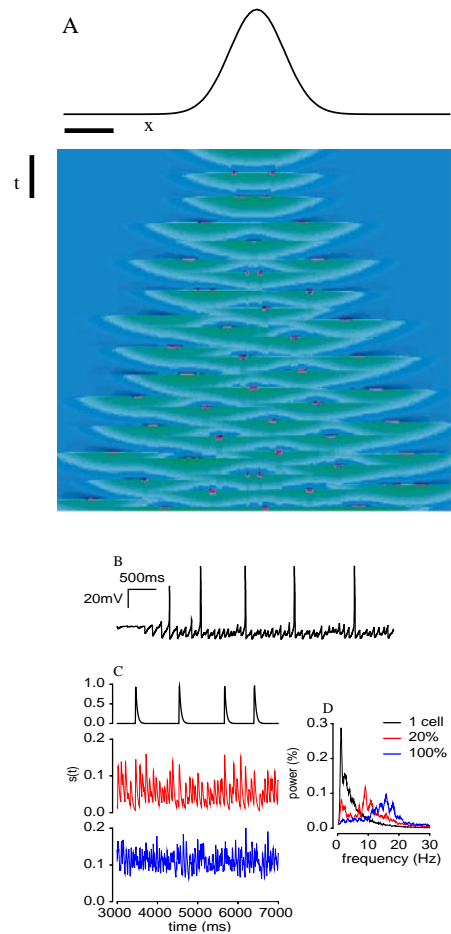
In our network model, the GABA$_A$-coupled cells have post-inhibitory rebound (PIR) properties and they are not oscillatory (when isolated) for any level of maintained input. A model neuron must be "released" from inhibition (or transiently depolarized) in order to produce a regenerative response. Our simulations are for a linear array of locally coupled cells, each of Hodgkin-Huxley type with a slowly inactivating T-type calcium current $I_{Ca\text{-}T}$ as the PIR mechanism (9). The duration of a rebound depolarization is about 30 to 50 ms, unless cut short by inhibition. Each cell generates a postsynaptic conductance in nearby cells with a decay time constant τ_{syn} of 40 ms and with weights whose spatial footprint is either on-center (Gaussian or square step profile) or off-center (reduced or zero weights near the center of the synaptic footprint).
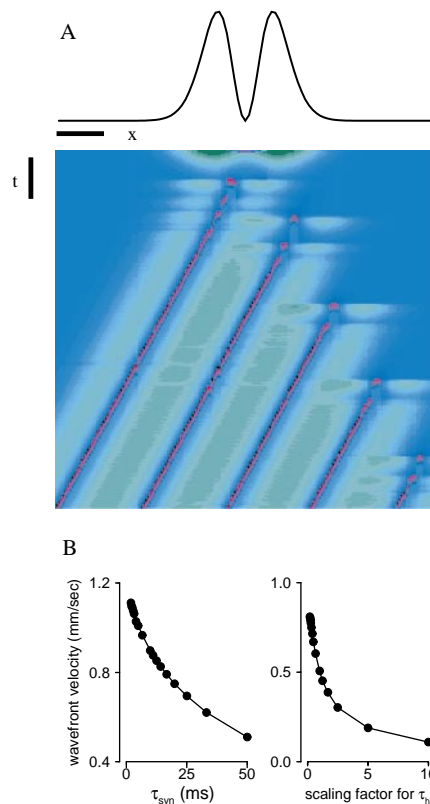
With on-center inhibition, local stimulation leads to discontinuous recruitment of activity throughout the network (Fig. 1A) (10). The activity persists with cells firing synchronously but only in spatially confined clusters, with cluster size of the same order of magnitude as the synaptic footprint's width. Visually, there is some spatiotemporal structure although it is not simple. Clusters do not appear as fixed in space, and successively firing clusters are spatially well separated. The PIR events are brief because of self-inhibition. Therefore cells must receive multiple cycles of brief inhibition in order to adequately prime their PIR mechanism to enable rebound upon release. Consequently, events in a given locale are also sparse in time. The recruitment into quiescent areas proceeds in a lurching manner; after a leading cluster fires, the next downstream firing is delayed by a cycle or more. The discrete progressive aspects show up in diagonal patterning throughout the medium. A cell's membrane potential time course (Fig. 1B) shows growing IPSPs during recruitment before the first rebound spike and highly chaotic fluctuations between spikes, generated completely by deterministic network dynamics. Activity, if summed on appropriate macroscopic spatial scales, looks approximately cyclic in time (Fig. 1, C and D). Target circuits or cells that employ larger convergence factors would receive higher effective frequencies from this network.

When synaptic interactions are off-center inhibitory, a different type of recruitment wave is seen, smoothly propagating but still very slow (Fig. 2A) (10). A localized initial stimulus (here, slightly asymmetric) can lead to lurching propagation mediated by cluster-type firing in one direction but smooth nearest neighbor progressive rebounding in the other. Firing durations here are longer than in the on-center case. The smoothly propagating successive cycles lead to periodic signaling across the medium. Such patterns can persist globally (as in Fig. 2A) or, for other parameters or even different initial conditions, the medium can exhibit transient lurching and smooth waves that seem to emerge randomly then disappear (11). The recruitment wave slows if cells experience or need longer hyperpolarization before they can rebound; for example, if either the synaptic time constant τ_{syn} or the time for PIR priming increases (Fig. 2B). When τ_{syn} is too small, synaptic inhibition becomes too brief to elicit postinhibitory rebound excitation, and the wave pattern disappears.

In some parameter regimes, a localized stimulus can initiate propagation of a single smooth PIR pulse (Fig. 3B) (10). Solitary

Fig. 1. Spatiotemporal activity with lurching recruitment waves in a mutually inhibitory network model with on-center coupling. The spatially localized holding stimulus is hyperpolarizing and primes the intracellular PIR mechanism so that PIR occurs at time $t = 0$, when the stimulus is released. (**A**) Color plots show membrane potential $V(x,t)$ (depolarization, red; rest, blue; hyperpolarization, green) of neurons with spatial location x along the horizontal axis ($0 \leq x \leq 2$ mm) and increasing t (ms) down the vertical axis. The spatial profile of synaptic weights is an on-center Gaussian curve (the curve above the color plot) with footprint width about one-tenth of the network's spatial extent. Default parameter values are used here (9). Initial conditions are as follows: $V(x,0) = V_{rest} = -66$ mV for each x except in the central region where $V(x,0) = -70$ mV for $0.9 \leq x \leq 1.1$; other variables at each location are initialized to their equilibrium values for the specified $V(x,0)$. Time bar, 200 ms; distance bar, 0.25 mm. (**B**) Membrane potential of a representative neuron. (**C**) Synaptic activation variable $s(t)$ of a single cell (black trace), averaged over 20% (red trace) or over the whole 100% (blue trace) of the neuronal population, with corresponding power spectra (**D**). The power spectra were computed by averaging over 10 trials, each with 4096 data points and a time bin of 5 ms.

Fig. 2. Off-center inhibition leads to both lurching and smoothly propagating recruitment waves. Default parameter values and localized stimulus are as in Fig. 1, except for an additional 2-mV hyperpolarization at $t = 0$ for $0.86 \leq x \leq 0.94$. Here, coupling is off-center inhibition (profile above the color plot); $\gamma = 1$. (**A**) From each leading cluster (isolated red spots) of the rightward-lurching recruitment wave emerges a smooth wave that travels slowly leftward, with a speed of 0.6 mm/s. The sustained repetitive pattern has a period of 800 ms. Time bar, 200 ms; distance bar, 0.25 mm. (**B**) The velocity of the leading smoothly propagating wave plotted against the inhibitory synaptic time constant τ_{syn} (left panel) or the scaling factor $1/\phi$ for the cellular time constant τ_h (right panel) of PIR recovery.
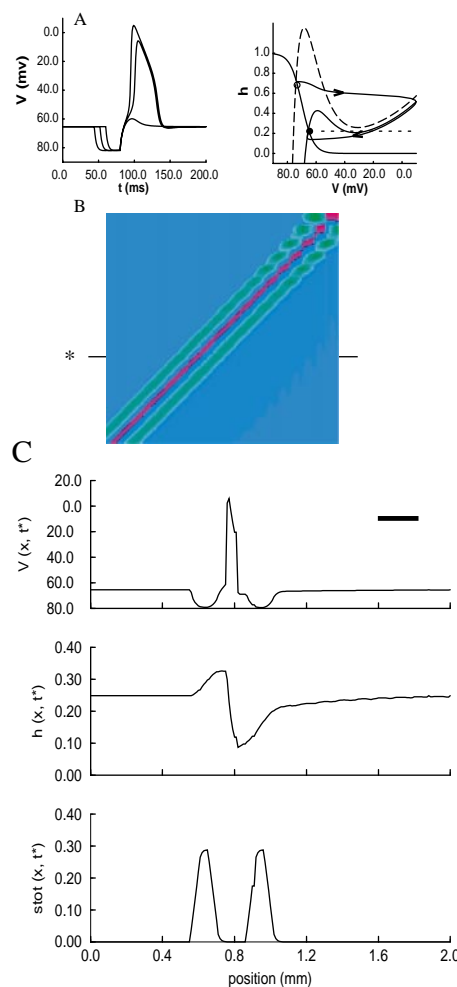
waves approaching from opposite directions into resting medium annihilate upon collision (*11*). Although the behavior appears reminiscent of an isolated action potential propagating along an axon, the mechanism is quite different (*12*). A major difference is that a PIR wave leaves a trail of synaptic inhibition in its wake. This trailing inhibition can promote a subsequent rebound event as it wanes (as in Fig. 2A). However, in Fig. 3B the time constant for synaptic decay is much smaller than that for repriming the PIR mechanism. The synaptic current dies away too quickly to produce an adequately prolonged inhibition for repriming (Fig. 3C). In contrast, slower synapses enable the hyperpolarized recovering cells to become extra-permissive, enough to be reexcited after the leading PIR event. The off-center inhibition leads to the double-humped profile of synaptic activity (Fig. 3C).

The cellular mechanism that underlies the PIR regenerative response depends on a fast autocatalytic process (in our case, rapid voltage-dependent activation of I_{Ca-T}) and a slower negative feedback process (slow inactivation of I_{Ca-T}) (*13*). Suppose that h

represents the relative suppressive influence, with $h = 0$ being maximally negating (at depolarized levels) and $h = 1$ being permissive (at very hyperpolarized levels); at rest, $h = h_{rest}$. To prime a neuron for rebounding requires sufficient hyperpolarization for a duration comparable to the time constant τ_h of the intrinsic PIR mechanism; this allows h to exceed h_{rest} by enough, so that h becomes adequately permissive (Fig. 3A). The neuron is then hyperexcitable and upon release it will rebound. In Fig. 3B, release occurs because of the gap in synaptic drive. Just before rebound, V rises slowly as the gap is first encountered (Fig. 3C). During the depolarized phase, h falls dramatically (its fall terminates the depolarization) to well below h_{rest}.

One can understand the constraints that dictate why PIR wave speed must be slow. In the network, a neuron receives inhibition from its surrounding neighbors weighted according to the synaptic footprint whose characteristic length is λ. If a PIR wave approaches a quiescent cell with speed c, the cell is inhibited for a time approximately λ/c and this time should exceed τ_h.

Thus, c must be small enough. Moreover, this simple bound (and the computed value of c, see Fig. 2B) decreases inversely with τ_h. For example, if λ = 100 μm and $\tau_h \sim 100$ ms then c must be less than a few millimeters per second, as in the case of lurching waves in the thalamic slice (*7, 8*). Such speeds are orders of magnitude slower than either the spread of population activity in networks driven by recurrent excitatory coupling (*14*) or axonal impulse propagation. The priming feature and its influence on speed contrasts substantially with the situation for axonal impulse propagation,
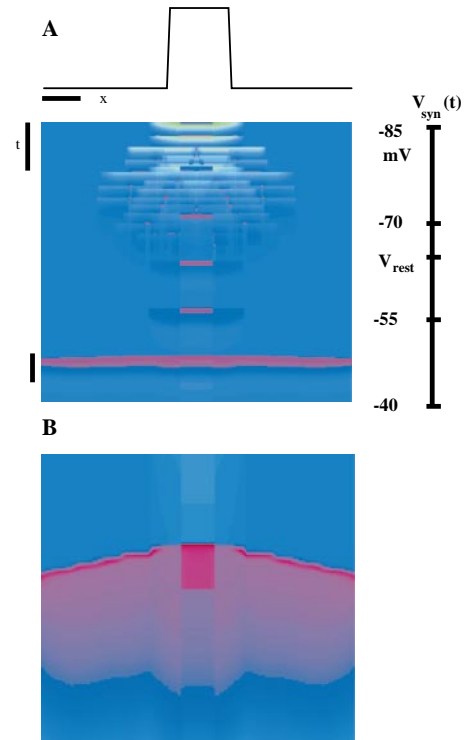
Fig. 3. Dynamic features of local and propagated solitary responses. (**A**) (left panel) Isolated neuron model shows rebound response upon release from hyperpolarizing current, provided current is adequately strong and of long enough duration. Parameters are adjusted from default values in order to enhance the gradeness of PIR response: $g_{Ca} = 0.75$ mS/cm^2 and $\tau_1 = 0$ ms (so that $\tau_h = 30$ ms); the initial condition is $V = -65$ mV and $h = 0.24$ for a holding current of 1 μA/cm^2. (Right panel) Representation of an isolated cell's PIR response in the $V - h$ phase plane. Thin solid curves are the V and h nullclines for the resting neuron (*21, 22*); their intersection (solid circle) represents the stable rest state at (h_{rest}, V_{rest}). For superposed hyperpolarizing input (net input current, -2.5 μA/cm^2) the V nullcline moves upward (dashed curve) and there is a new hyperpolarized steady state (open circle); here, h is more permissive than at rest ($h = h_{rest}$). The thick curve with arrowheads is the $V - h$ trajectory of the PIR response after release of the input current. (**B**) A solitary smooth wave propagates from a locally stimulated region. The off-center footprint has a square step profile (λ = 200 μm and λ$_{gap}$ = 100 μm). Similar results are found for off-center Gaussian synaptic weights. The model with default parameter settings does not support a solitary wave. Here, parameter values that differ from the default are as follows: $\tau_1 = 800$ ms, $g_{syn} = 2.5$ mS/cm^2, and $k_f = 1$ (ms)$^{-1}$, $k_r = 0.1$ (ms)$^{-1}$. Initial conditions are as in Fig. 1, translated to the right end. (**C**) Spatial profiles of V, h, and s_{tot} at $t^* = 1000$ ms [thin horizontal line, marked by the asterisk in (B)] for the solitary traveling pulse in (B). The heavy bar indicates 200 ms.

Fig. 4. Change in sign of GABAergic synapses converts slow lurching recruitment by inhibition to nearly instantaneous propagation of the depolarizing event. Parameter values are as in Fig. 1, except that here the on-center footprint has a square step profile. (**A**) The medium is stimulated periodically in time with a square pulse of current (30 μA/cm^2, 50 ms) over the centered region: $0.9 \leq x \leq 1.1$. The linear ramp of $V_{syn}(t)$ (15 mV/s) simulates increasing intracellular chloride concentration. Time bar, 500 ms; distance bar, 0.25 mm. The early phase of response shows lurching waves and irregular cluster firings as in Fig. 1A. The medium is inexcitable during the middle phase when V_{syn} is close to V_{rest}; synapses are only shunting. When GABA$_A$ synapses are adequately depolarizing from the resting state, recruitment spreads rapidly ($\sim$25 times faster than lurching waves), with near-simultaneous firing in response to the depolarizing stimulus. If V_{syn} were to increase even more, the neurons would steadily depolarize. (**B**) Magnification of 320-ms time window as indicated by the vertical bar in (A) shows the fast propagation event.

where the slower time scales of membrane recovery (like the gating time constant of the delayed rectifier potassium current) hardly influence conduction speed (*12*).

The possibility that PIR activity may propagate smoothly depends crucially on the interaction between the intracellular (intrinsic) and the intercellular (network) features of our model. If each neuron is rebound-excitable but does not oscillate for maintained input, then the off-center profile of the synaptic weight footprint is important. Without this spatial gap in the inhibitory spread, the essential requirement for space-time translation invariance of a traveling wave cannot be met. Imagine the time course of a neuron during a rebound event. The depolarizing phase is preceded by hyperpolarization and then begins when the cell is released from the $GABA_A$-mediated synaptic input. If this temporal trajectory is to be interchangeable with the spatial profile (as in Fig. 3C), then the locale under a depolarized regime must not be inhibited. This implies no inhibition of self, and by continuity, of nearest neighboring cells, which is an off-center profile for inhibition (*15*). The narrower this footprint's gap is, the slower is propagation, and if it is too narrow propagation will be precluded.

The substantial differences between the inhibition-induced recruitment that we have shown and the well-known excitation-driven waves may be directly demonstrated with our model. By dynamically modulating the reversal potential V_{syn} of the $GABA_A$ synapses, the synaptic current's sign may be changed, as occurs in the circadian pacemaker network or during development or high activity (*16*). To illustrate the dramatic effects of such modulation, we slowly increase V_{syn} (from 20 mV below resting potential as in Figs. 1 through 3) while locally stimulating the network with brief depolarizing pulses every 500 ms. Using on-center synaptic weights, the activity evolves from spatially localized rebound clustering to quiescence and unresponsiveness when V_{syn} is near V_{rest} and synapses are truly shunting (Fig. 4) (*10*). Ultimately, the network gains excitability and the next brief stimulus leads to very rapid propagation of a depolarization wave, with no pre- or posthyperpolarization in the voltage time course. The propagation speed of this event is 25 times faster than that of the smooth PIR wave in Fig. 2A, causing nearly synchronous discharge of the network. A special feature of our rather simple model enables this behavior. At rest, our model's PIR process is partially primed: h_{rest} is not near zero (Fig. 3A). Consequently, the spike generator is not totally disabled. The system is excitable and it responds regeneratively to a brief depolarization.

Thus when V_{syn} exceeds V_{rest} sufficiently, this excitability is capable of supporting fast long-range communication via local excitatory but near-shunting interactions.

Our finding that localized coupling architecture determines the propagation mode has implications for the thalamic system. Multiple electrode recordings in slices indicate lurching propagation (*7*) with no reported evidence for smooth waves (although we urge the use of imaging methods whose finer spatial resolution would provide more direct and conclusive evidence). Therefore, based on computations with our idealized model and with a more complete two-layer RE-TC model (*17*), we suggest that functional coupling in the disynaptic pathway TC-RE-TC is effectively on-center. Consistent with this suggestion, return EPSPs and IPSPs are sometimes seen when individual RE or TC cells, respectively, are stimulated (*18*). Direct support for autaptic synapses or the footprint shape of localized coupling, although present in some systems (*19*), is not yet available for the thalamic circuitry. Our results would also apply to an isolated RE subsystem (a thalamic slice in which RE-RE, but not RE-TC-RE, coupling was operative) if experimental conditions were adjusted so that RE cells responded to IPSP barrages with rebound bursts (*20*).

Our results provoke broader speculation about functional implications for distributed networks of GABAergic PIR neurons. The regularity of the slow smooth wave trains (Fig. 2) suggests utility for a central pattern generator, for example, for driving slow undulatory motion. It is a challenge to account for the emergence of pattern or computational ability on long time scales based on cellular mechanisms with much shorter time scales. Such slow waves might be employed in applications requiring long-delayed dynamic memory. In analogy to how the auditory system identifies the location of sound sources, slow propagation on delay lines could be used for detection of events that are temporally separated by hundreds to thousands of milliseconds. Whether the slow recruitment and maintained inhibition-mediated patterns seen here can still arise in networks having some degree of recurrent excitation will require additional study. Regardless, the different spatiotemporal patterns become signatures for identifying qualitative intrinsic and circuit properties even in isolated networks.

REFERENCES AND NOTES

1. D. H. Perkel and B. Mulloney, *Science* **185**, 181 (1974); R. A. Satterlie, *ibid.* **229**, 402 (1985); E. Marder and R. L. Calabrese, *Physiol. Rev.* **76**, 687 (1996).
2. For the hippocampus, see T. F. Freund and G. Buzsàki, *Hippocampus* **6**, 345 (1996); for the neocortex, see Z. F. Kisvárday, C. Beaulieu, U. T. Eysel, *J. Comp. Neurol.* **327**, 398 (1993); for the thalamus, see (*3*).
3. M. Steriade and M. Deschenes, *Brain Res. Rev.* **8**, 1 (1984); M. von Krosigk, T. Bal, D. A. McCormick, *Science* **261**, 361 (1993).
4. M. A. Whittington, R. D. Traub, J. G. R. Jeffreys, *Nature* **373**, 612 (1995); X.-J. Wang and G. Buzsàki, *J. Neurosci.* **16**, 6402 (1996).
5. X.-J. Wang and J. Rinzel, *Neural Computation* **4**, 84 (1992); *Neuroscience* **53**, 899 (1993); C. van Vreeswijk, L. F. Abbott, G. B. Ermentrout, *J. Comput. Neurosci.* **1**, 313 (1995); D. Terman, N. Kopell, A. Bose, *Physica D*, in press; A. A. Sharp, F. K. Skinner, E. Marder, *J. Neurophysiol.* **76**, 867 (1996).
6. S. M. Sherman and R. W. Guillery, *J. Neurophysiol.* **76**, 1367 (1996).
7. U. Kim, T. Bal, D. A. McCormick, *ibid.* **74**, 1301 (1995).
8. D. Golomb, X.-J. Wang, J. Rinzel, *ibid.* **75**, 750 (1996); A. Destexhe, T. Bal, D. A. McCormick, T. J. Sejnowski, *ibid.* **76**, 2049 (1996).
9. Each neuron is endowed with a T-type low-threshold calcium current I_{Ca-T} and a leak current I_L. The current balance equation is $C_m dV(x,t)/dt = -I_L - I_{Ca-T} - g_{syn}s_{tot}(x,t)[V(x,t) - V_{syn}]$. We have $I_L = g_L(V - V_L)$; $I_{Ca-T} = g_T m_\infty(V)h(V - V_{Ca})$, $m_\infty = 1/[1 + exp(-(V + 40)/7.4)]$, $dh/dt = \phi[h_\infty(V) - h]/\tau_h(V)$ with $h_\infty(V) = 1/[1 + exp((V + 70)/4)]$, $\tau_h(V) = \tau_0 + \tau_1/(1 + exp((V + 50)/3))$, and $\phi = 1.3$ is a scaling factor for τ_h. The total synaptic drive is $s_{tot}(x,t) = \int w(x - y)s(y,t)dy$, where the distance-dependent connectivity footprint $w(x) = A exp(-x^2/\lambda^2)[1 - \gamma exp(-x^2/\lambda_{gap}^2)]$ with $\lambda = 200$ μm, $\lambda_{gap} = 140$ μm, and A is chosen such that $\int w(x)dx = 1$; $\gamma = 0$ if the coupling is on-center. In the text, "footprint width" and "gap width" refer to the lengths 2λ and $2\lambda_{gap}$, respectively. The gating variable for the synaptic current $s(x,t)$ obeys a first-order kinetics [see Wang and Rinzel (*5*)], $ds/dt = k_f s_\infty(V_{pre})(1 - s) - k_r s$, where $s_\infty(V) = 1/\{1 + exp[-(V + 35)/2]\}$, $k_f = 0.5$ and $k_r = 0.025$ [in (ms)$^{-1}$]; $\tau_{syn} = 1/k_r$]. Other used parameter values are $C_m = 1$ μF/cm^2; $\tau_0 = 30$, and $\tau_1 = 500$ (in ms); $g_L = 0.4$, $g_{Ca-T} = 1.5$, and $g_{syn} = 5$ in mS/cm^2; $V_L = -70$, $V_{Ca} = +90$ and $V_{syn} = -85$ (in mV). For numerically solving the model's equations, we approximate the continuum formulation by discretizing in space, using N cells equally distributed along the network's length L (arbitrarily chosen as 2 mm); $N = 200$ unless stated otherwise. The spatially discretized version is numerically integrated in time using a second-order modified-Euler method with $\delta t = 0.5$ ms. Accuracy was confirmed by achieving agreement after adequately refining the temporal and spatial discretizations.
10. The model's spatiotemporal activity can be dynamically visualized over the Internet by using an MPEG-capable browser, opening the Web site http://www.pitt.edu/~phase, and going to the section "Movies of waves in a simple PIR inhibitorily coupled network."
11. J. Rinzel, D. Terman, X.-J. Wang, B. Ermentrout, data not shown.
12. During an axonal action potential's upstroke, the slower negative feedback processes (such as inactivation of the sodium current or activation of some potassium currents) remain approximately at their resting values. In PIR, the negating state of such slower feedback processes must be reduced from resting levels by prehyperpolarizing the membrane so that rebounding can occur (*3, 7, 8*). This feature intimately involves the kinetics of negative feedback in the rebound upstroke. Also, a spatially symmetric and localized depolarization on an axon typically yields just two impulses, one propagating away in each direction. In striking contrast, for PIR, release from a localized and symmetric initial hyperpolarization can lead to widespread maintained activity, behind the recruitment front.
13. The behaviors shown here do not require I_{Ca-T} per se. Because PIR is qualitatively equivalent to anodal break excitation, there is a class of membrane models that when used in a network formulation like ours show activity patterns as reported here. We have found slow lurching and smooth waves by using a Morris-Lecar-type action potential model [see (*21*)] that has a fast, non-inactivating, inward current and slower outward current (*11*).

14. R. D. Chervin, P. A. Pierce, B. W. Connors, *J. Neu-rophysiol.* **60**, 1695 (1988); R. Miles, R. D. Traub, K. S. Wong, *ibid.*, p. 1481; D. Golomb and Y. Amitai, *ibid.* **78**, 1199 (1997).

15. We note however that smooth waves are possible with on-center synaptic coupling if individual neurons are able to oscillate for some appropriate levels of maintained input (*10*).

16. S. Wagner, M. Castel, H. Gainer, Y. Yarom, *Nature* **387**, 598 (1997); E. Cherubini, J. L. Gaiarsa, Y. Ben-Ari, *Trends Neurosci.* **14**, 515 (1991); K. J. Staley, B. L. Soldo, W. R. Proctor, *Science* **269**, 977 (1995).

17. Using the more complete thalamic model of Golomb *et al.* (*8*), G. Smith and J. Rinzel found (data not shown) footprint-dependent propagation modes. Lurching occurs with on-center footprints. But smooth waves are possible if the effective TC-RE-TC coupling is off-center; for example, if the RE-TC inhibition is off-center while the excitation from TC to RE is narrowly focused on-center.

18. T. Bal, M. von Krosigk, D. A. McCormick, *J. Physiol.* **483**, 665 (1995); U. Kim, M. V. Sanchez-Vives, D. A. McCormick, *Science* **278**, 130 (1997); F.-S. Lo and S. M. Sherman, *Exp. Brain Res.* **100**, 365 (1994).

19. G. Tamas, E. H. Buhl, P. Somogyi, *J. Neurosci.* **17**, 6352 (1997); A. M. Thomson and J. Deuchars, *Trends Neurosci.* **17**, 119 (1994).

20. M. V. Sanchez-Vives and D. A. McCormick [*J. Neurosci.* **17**, 8894 (1997)] report that under normal slice conditions they do not see rebounding in RE cells due to RE-RE GABA$_A$ barrages. D. Ulrich and J. R. Huguenard [*J. Neurophysiol.* **78**, 1748 (1997)] have demonstrated rebounding with injection to the RE cell's soma of dynamic-clamp simulated GABA$_A$ currents.

21. J. Rinzel and G. B. Ermentrout, in *Methods in Neuronal Modeling: From Synapses to Networks*, C. Koch and I. Segev, Eds. (MIT Press, Cambridge, MA, 1989, pp. 135–169).

22. Elements of phase plane analysis for excitable membrane systems can be found in R. FitzHugh, *Biophys. J.* **1**, 445 (1961) and in (*21*). For a two-variable system the nullclines are the two curves in the phase plane along which either variable has zero velocity. In our case, from the differential equations, setting $dV/dt = 0$ gives the V nullcline as $h = [g_L(V - V_L) - I_{app}]/[g_{Ca-T}m_\infty(V)(V_{Ca} - V)]$ and similarly the h nullcline as $h = h_\infty(V)$. For default parameter values, the steady state for any I_{app} is on the left branch and is therefore stable.

23. Supported by the Alfred P. Sloan Foundation, NSF grants DMS-9203299 and DMS-9626728, NIH grants MH53717-01 and MH 47150, and the W. M. Keck Foundation.

15 August 1997; accepted 15 January 1998

Linkage of Adhesion, Filamentous Growth, and Virulence in *Candida albicans* to a Single Gene, *INT1*

Cheryl A. Gale, Catherine M. Bendel, Mark McClellan, Melinda Hauser, Jeffrey M. Becker, Judith Berman,* Margaret K. Hostetter*

Adhesion and the ability to form filaments are thought to contribute to the pathogenicity of *Candida albicans*, the leading cause of fungal disease in immunocompromised patients. Int1p is a *C. albicans* surface protein with limited similarity to vertebrate integrins. *INT1* expression in *Saccharomyces cerevisiae* was sufficient to direct the adhesion of this normally nonadherent yeast to human epithelial cells. Furthermore, disruption of *INT1* in *C. albicans* suppressed hyphal growth, adhesion to epithelial cells, and virulence in mice. Thus, *INT1* links adhesion, filamentous growth, and pathogenicity in *C. albicans* and Int1p may be an attractive target for the development of antifungal therapies.

Candida albicans is the leading cause of invasive fungal disease in premature infants, diabetics, surgical patients, and hosts with human immunodeficiency virus infection or other immunosuppressed conditions. Despite appropriate therapy, mortality resulting from systemic *C. albicans* infection in immunocompromised patients approaches 30% (*1*). The pathogenesis of *C. albicans* infection is postulated to involve adhesion to host epithelial and endothelial cells and morphologic switching of yeast cells from the ellipsoid blastospore to various filamentous forms: germ tubes, pseudohyphae, and hyphae (*2*).

The *C. albicans* gene *INT1* was originally cloned because of its similarity to vertebrate leukocyte integrins (*3*), adhesins that bind extracellular matrix proteins and induce morphologic changes in response to extracellular signals (*4*). *INT1* expression in the budding yeast *S. cerevisiae* triggers a morphologic switch to filamentous growth (*3*). In *C. albicans*, multiple adhesins mediate attachment to epithelium, endothelium, or platelets (*5–8*). Because laboratory strains of *S. cerevisiae* have few adhesins (*7*), we investigated whether Int1p is present on the cell surface and can function as an adhesin when it is expressed in *S. cerevisiae*.

When intact *S. cerevisiae* cells expressing *INT1* were treated with an impermeant biotinylation reagent, Int1p became biotin-labeled, indicating that at least one portion of Int1p was on the exterior cell surface (Fig. 1A). Nonsurface proteins, such as Rap1p, an abundant nuclear protein, were not biotinylated (Fig. 1A). *Saccharomyces cerevisiae* cells expressing *INT1* (strain YCG101) ad-

hered to monolayers of human cervical epithelial cells (HeLa), whereas *S. cerevisiae* cells carrying vector sequences (YCG102) and YCG101 cells grown in glucose [to repress Int1p expression from the *GAL10* promoter (*9*)] did not adhere to HeLa monolayers (Fig. 1B). Furthermore, adhesion of YCG101 cells to HeLa monolayers was specific for Int1p epitopes: UMN13, a polyclonal antibody recognizing Int1p amino acids 1143 to 1157 [a region predicted to be extracellular (*3*)], inhibited adhesion, whereas nonimmune rabbit immunoglobulin G (IgG) did not (Fig. 1B). Thus, the expression of Int1p alone was sufficient to confer adhesive capacity on *S. cerevisiae*.

INT1 expression induces the growth of highly polarized buds (*3*). To test the possibility that the increased surface area of polarized *S. cerevisiae* cells (Fig. 1C) influences cell adhesion, we performed adhesion assays with a *cdc12-6*^{ts} strain (JKY81-5-1) (*10*) that forms multiple elongated buds at the permissive temperature (*11*) (Fig. 1C). Adhesion of the *cdc12-6*^{ts} strain to HeLa cell monolayers did not differ from that of YCG102 and was significantly less than the adhesion seen upon expression of *INT1* (Fig. 1B), indicating that filamentous morphology alone is not sufficient to explain the increased adhesion of *INT1*-expressing cells.

We next tested the hypothesis that *INT1* is involved in adhesion and filamentous growth in *C. albicans* as well. Both copies of *INT1* were disrupted sequentially in *C. albicans* strain CAI4 (*12*) by means of a *hisG-CaURA3-hisG* cassette (*13*) yielding a Ura$^+$ *int1/INT1* heterozygote (CAG1) and a Ura$^+$ *int1/int1* homozygote (CAG3). *INT1-CaURA3* was reintegrated into the genome of a Ura$^-$ *int1/int1* homozygote (CAG4) to yield the *int1/int1 + INT1* heterozygous reintegrant (CAG5) (*14*), which served as an *int1/int1 + INT1* Ura$^+$ control to ensure that CAG3 phenotypes could be attributed to disruption of *INT1*.

The specific adhesion of the *C. albicans int1/int1* strain (CAG3) to HeLa cells was

C. A. Gale, Department of Pediatrics, University of Minnesota, 420 Delaware Street S.E., Minneapolis, MN 55455, USA, and Department of Plant Biology, University of Minnesota, 220 Biological Sciences Center, St. Paul, MN 55108, USA.
C. M. Bendel, M. McClellan, M. K. Hostetter, Department of Pediatrics, University of Minnesota, 420 Delaware Street S.E., Minneapolis, MN 55455, USA.
M. Hauser and J. M. Becker, Department of Microbiology, University of Tennessee, M409 Walters Life Sciences, Knoxville, TN 37996, USA.
J. Berman, Department of Plant Biology, University of Minnesota, 220 Biological Sciences Center, St. Paul, MN 55108, USA.

*To whom correspondence should be addressed. E-mail: judith@biosci.cbs.umn.edu and hoste001@maroon.tc.umn.edu